Cement and Concrete Composites 115 (2021) 103857

Contents lists available at ScienceDirect

Cement and Concrete Composites

journal homepage: http://www.elsevier.com/locate/cemconcomp

Mechanical performance of MgO-doped Engineered Cementitious Composites (ECC)

Haoliang Wu [a,b,c], Jing Yu [d,e,f], Yanjun Du [c], Victor C. Li [a,*]

[a] Department of Civil and Environmental Engineering, University of Michigan, Ann Arbor, USA
[b] Department of Civil and Environmental Engineering, Hong Kong University of Science and Technology, Hong Kong, China
[c] Jiangsu Key Laboratory of Urban Underground Engineering & Environmental Safety, Southeast University, Nanjing, PR China
[d] School of Civil Engineering, Sun Yat-Sen University, Guangzhou, PR China
[e] Guangdong Key Laboratory of Oceanic Civil Engineering, Guangzhou, PR China
[f] Southern Marine Science and Engineering Guangdong Laboratory, Zhuhai, PR China

ARTICLE INFO

Keywords:
Magnesia
Engineered cementitious composite (ECC)
Strain-hardening cementitious composite (SHCC)
Compressive strength
Tensile performance
Water permeability
Fiber-matrix interface

ABSTRACT

Engineered Cementitious Composites (ECC) is a special class of high performance cement-based composites featuring high tensile deformation capacity (>2%) and tight crack opening (typically <100 μm). It is reported that doping ECC with a small proportion of reactive magnesia (MgO) can significantly enhance the water impermeability and self-healing performance. However, the present knowledge on how the MgO affects the mechanical performance of ECC is very limited. In this investigation, the influence of MgO (0–10% by weight of cement) on the workability, compressive strength, crack pattern, water permeability and tensile performance of the MgO-doped ECC were comprehensively evaluated. It was concluded that a higher MgO proportion yielded higher/better tensile strength, crack control capacity, water impermeability and workability, though it also led to slightly lower compressive strength, elastic modulus and fracture toughness in ECC. Additionally, doping 6% MgO in ECC was found to be optimal for enhancing the tensile deformation capacity, which is consistent with the prediction from the micromechanical model. These findings shed light on the design of sustainable ECC in the future.

1. Introduction

Engineered Cementitious Composites (ECC) is a class of high-performance composites featuring high tensile deformation capacity and tight crack opening [1–5]. Specially, ECC shows ultimate tensile strain hundreds of times larger than that of plain concrete [6–8], and the opening of the multiple cracks is typically limited to below 100 μm. According to the literature, the self-controlled tight crack opening of ECC is helpful to enhance the self-healing capacity and to resist the penetration of aggressive agents into the concrete cover of reinforced concrete structures, which leads to improved structural durability and service life [9–12]. The outstanding durability and properties make ECC attractive for construction applications such as bridge deck link slab, renovation engineering, and pavement and hydraulic structures [13–17]. Nevertheless, the large dosage of cement in ECC generally leads to high carbon emissions and energy consumption [15–18]. Therefore, replacing cement by supplementary cementitious materials has received attentions from researchers [19].

In recent decades, reactive magnesia (MgO) as an expansive addition for mass concrete in dam construction was used to control shrinkage [20–24]. Previous studies have also reported that the addition of MgO can lead to high resistance to chemical attacks [25,26] and enhance the water impermeability of concrete, as the hydration products of MgO including magnesium silicate hydrate, hydrotalcite-like phases and brucite ($Mg(OH)_2$) can effectively densify the matrix [11,27–29]. Moreover, adding MgO in the binder can lower the carbon footprint associated with cement manufacture [21–24,30–34]. To extend the service life of infrastructures, Wu et al. [11,12], have explored the water permeability and self-healing properties of MgO-doped ECC under different exposure conditions including tap water and acid mine drainage. Despite the excellent water impermeability and self-healing performance of the MgO-doped ECC, the present knowledge on how MgO affects the mechanical performance of ECC is limited.

This study aims to experimentally explore the influence of MgO

* Corresponding author.
E-mail address: vcli@umich.edu (V.C. Li).

https://doi.org/10.1016/j.cemconcomp.2020.103857
Received 17 April 2020; Received in revised form 13 September 2020; Accepted 18 October 2020
Available online 20 October 2020

Table 1
Mix design of MgO-doped ECC (in weight ratio).

Series	Mix ID	Cement	MgO	FA	Sand/binder	Water/binder	SP[a]/binder	PVA Fiber[b]	Flow time[c] (s)	Flow diameter (mm)
E1.2	0%E1.2	1	0	1.2	0.36	0.25	0.32%	2%	28.2	205
	4%E1.2	0.96	0.04	1.2	0.36	0.25	0.45%	2%	29.1	201
	6%E1.2	0.94	0.06	1.2	0.36	0.25	0.56%	2%	27.8	210
	8%E1.2	0.92	0.08	1.2	0.36	0.25	0.86%	2%	27.5	208
	10%E1.2	0.90	0.10	1.2	0.36	0.25	1.13%	2%	28.3	205
E2.2	0%E2.2	1	0	2.2	0.36	0.25	0.25%	2%	26.4	209
	4%E2.2	0.96	0.04	2.2	0.36	0.25	0.37%	2%	25.7	212
	6%E2.2	0.94	0.06	2.2	0.36	0.25	0.48%	2%	26.8	208
	8%E2.2	0.92	0.08	2.2	0.36	0.25	0.74%	2%	27.1	200
	10%E2.2	0.90	0.10	2.2	0.36	0.25	0.98%	2%	27.3	209

[d] Flow diameter was obtained from the mini-slump cone.
[a] SP refers to polycarboxylate-based superplasticizers.
[b] PVA fiber proportion is by volume.
[c] Flow time was obtained from the modified Marsh cone.

Table 2
Chemical compositions of cement, MgO and fly ash.

Materials[a]	SiO_2 (%)	Al_2O_3 (%)	SO_3 (%)	MgO (%)	P_2O_5 (%)	K_2O (%)	TiO_2 (%)	Fe_2O_3 (%)	CaO (%)	Cl (%)	LOI[b] (%)
Cement	19.19	15.4	2.54	3.46	–	0.07	0.39	2.13	54.79	-	2.03
MgO	0.31	0.2	–	95.76	–	–	0.01	0.13	0.81	0.03	2.75
Fly ash	38.56	17.92	1.86	4.35	1.12	0.97	1.24	9.27	20.92	0.01	3.78

[a] Chemical composition was analyzed by ARL9800XP + XRF spectrometry.
[b] LOI: Loss on ignition.

(0–10% by weight of cement) on the mechanical performance of the MgO-doped ECC, in term of workability, compressive strength, crack pattern, water permeability and tensile properties. Micromechanical parameters including matrix fracture toughness, interfacial frictional bond, interfacial chemical bond, and slip hardening coefficient were also experimentally determined. Micromechanics served to link the composite mechanical performance to the micromechanical parameters of material. This study reveals the mechanisms behind macroscale property improvements resulting from the doping of ECC with MgO.

2. Basics of the micromechanical model

Robust tensile strain-hardening in ECC relies on the steady propagation of multiple micro-cracks initiated from the defects in matrix under tension [2]. According to the micromechanical model, two criteria must be fulfilled to ensure a successful design of ECC. The strength criterion and energy criterion are shown in Eq. (1) and Eq. (2), while more information can be found in Li [2].

$$\sigma_0 > \sigma_{fc} \tag{1}$$

$$J_b' \equiv \sigma_0\delta_0 - \int_0^{\delta_0} \sigma(\delta)d\delta > J_{tip} \cong K_m^2/E_m \tag{2}$$

Additionally, the pseudo-strain-hardening (PSH) indices (Eqs. (3) and (4)) were introduced to quantify the strain-hardening potential in ECC [31]. To obtain robust tensile strain-hardening, the PSH (strength) and PSH (energy) were recommended to be no less than 1.45 and 3.0 [35], respectively.

$$\text{PSH (strength)} = \sigma_0/\sigma_{fc} \tag{3}$$

$$\text{PSH (energy)} = J_b'/J_{tip} \tag{4}$$

3. Materials and methods

3.1. Materials and mix design

Table 1 lists the mix proportions of ECC. Type I Portland cement (PC, ASTM C150 [36]), Class F fly ash (FA, ASTM C618 [37]), and light burned MgO were adopted as binder materials. The light burned MgO with a purity of 95.76% and reactivity of 105s was calcined in 900 °C

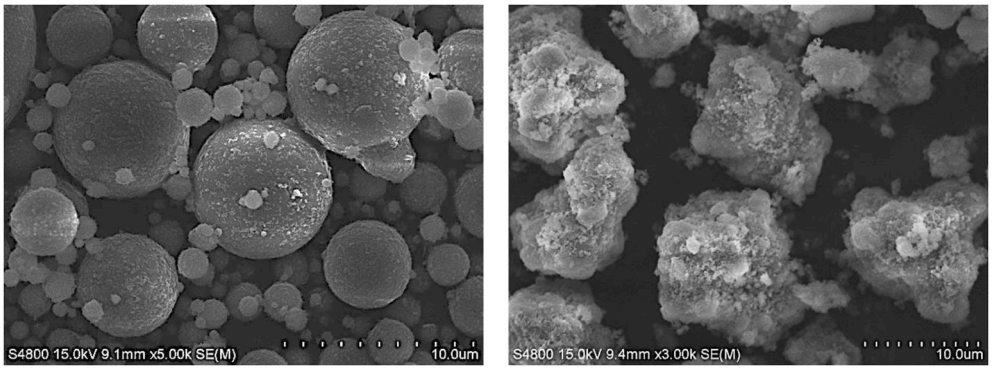

Fig. 1. SEM pictures of (left) fly ash and (right) MgO powder.

Table 3
Nominal properties of PVA fiber.

Diameter (μm)	Length (mm)	Fiber strength (MPa)	Young's modulus (GPa)
39	8	1600	42.8

(MAGOX® premium grade). The doping proportion of MgO was 0–10% by weight of the cement. Table 2 shows the chemical compositions of binder materials, and Fig. 1 shows the morphology of FA and MgO powders. The average size of the fine silica sand was 75 μm. The polyvinyl-alcohol (PVA) fiber was sourced from Kuraray Co., Ltd in Japan. Fiber nominal properties are listed in Table 3. In this study, two series of ECC mixes with the FA/(PC + MgO) ratios of 1.2 and 2.2 were explored. The water/binder ratio were 0.25, and the PVA fiber content was 2% by volume, which is a typical value for ECC. Polycarboxylate-based superplasticizers (SP) was used to control the workability of these mixes.

3.2. Sample preparation

A 12-L mortar mixer was used to prepare ECC. The mixing progress was as follow: (1) the PC, FA, MgO and silica sand were dry mixed for approximately 3 min at 100 rpm; (2) water with SP were added and mixed with the solid for 5 min at 100 rpm to obtain a homogeneous mixture; and (3) the PVA fibers were added and mixed for another 5 min at 100 rpm to obtain uniform fiber distribution.

The fresh mixtures were cast into stainless molds for compression and tension tests. Plastic sheets were used to cover all the specimens for 24 h before demolding. The demolded specimens were then stored for 27 days in the curing room, where the relative humidity and temperature were set at 65 ± 5% and 20 ± 2 °C, respectively.

3.3. Testing methods

The Marsh cone and mini-slump flow tests were used to determine the fresh properties as suggested in Ref. [38]. The Marsh cone was a 1700-mL plastic funnel with the internal opening diameter of 20 mm. The flow time of ECC mixture was recorded after all the material flow out from the bottom opening. For the mini-slump flow test, the truncated cone (height of 60 mm, bottom diameter of 100 mm and top diameter of 70 mm) was filled with the fresh mixture and immediately lifted upward. The flow diameter was measured when the moving of the mixture stopped. Both tests were repeated twice to get an average value.

Compressive strength was measured by 50-mm cubic specimens with the loading speed of 0.54 ± 0.18 MPa/s as per ASTM C109/C109 M [39].

Based on the relative density (ρ_s) and dry density (ρ_d) of the specimens, the porosity (n) of specimens was calculated based on Equation (5) – (6):

$$n = e/(1+e) \tag{5}$$

$$e = \frac{\rho_s}{\rho_d} - 1 \tag{6}$$

Dumbbell specimens were used for the tension test (Fig. 2), as suggested by the Japan Society of Civil Engineer (JSCE) [40]. The tensile test was conducted with a 10-kN Instron® instrument with the loading speed of 0.5 mm/min. The deformation was measured by a pair of linear variable displacement transduces in the middle 80-mm region. After the tension test, one middle line was drawn on the dumbbell specimen in the longitudinal direction. Then the residual crack pattern within the middle 80-mm region were analyzed along the line with an optical electron microscope (infinity X–C21) with the resolution of 10 μm.

A falling head system (Fig. 3) was used in the permeability test as suggested by Lepech and Li [6]. A cuboid-shaped plexiglass water tank was used to clamp the dumbbell specimen. In this setup, the inner-size of the cross-section of water tank was designed to fit the middle part of the dumbbell specimen. Rubber seals were used to ensure the water-tightness. More details on the calculation of water permeability coefficient can be found in Ref. [11].

The fracture toughness of matrix (K_m) was obtained from the three-point fracture bending test as per ASTM E399 [41]. The K_m specimens were prepared without fiber and cast into a beam mold (304.8 mm × 38.1 mm × 76.2 mm). The loading span between supports was 254.0 mm. The notch depth to height ratio was kept at 0.4. The Young's modulus E_m and first cracking strength σ_{fc} were determined from the uniaxial tension test. E_m refers to the slope of the initial linear part of the

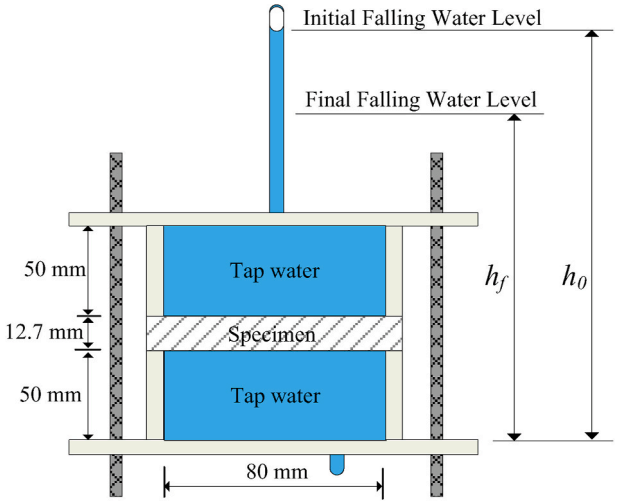

Fig. 3. Falling head water permeability testing setup.

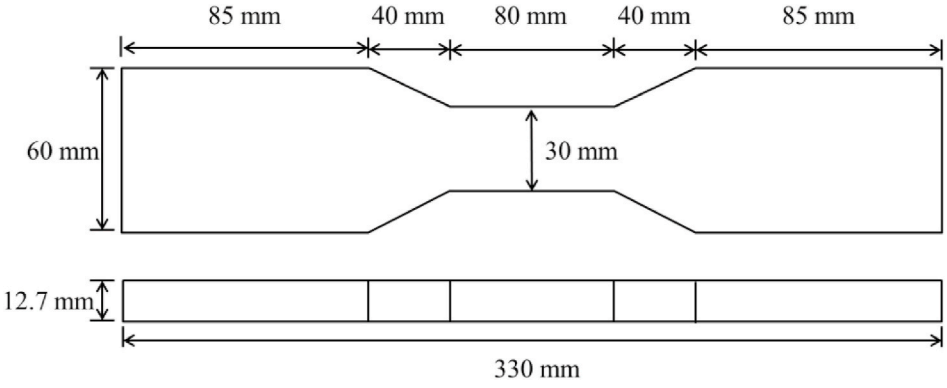

Fig. 2. Dumbbell specimen for tension as per JSCE [40].

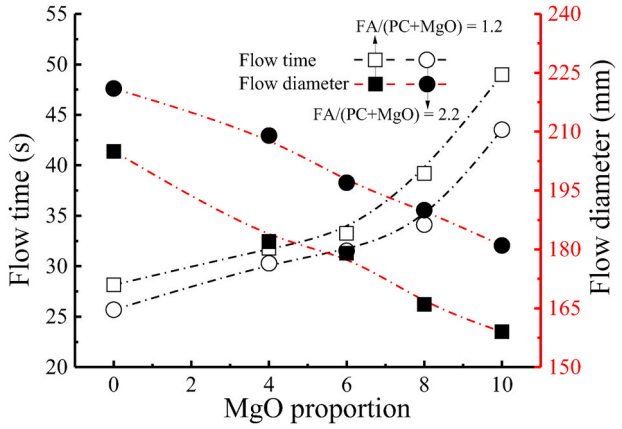

Fig. 4. Effective of MgO proportion on flow time and flow diameter for mixes with a fixed amount of superplasticizer (0.32% by weight of binder).

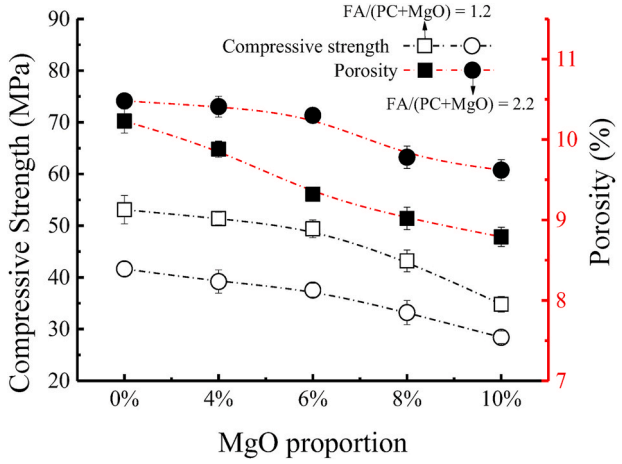

Fig. 5. Effect of MgO proportion on ECC compressive strength and porosity.

stress-strain curve, and σ_{fc} refers to the stress at the first cracking [40]. Single fiber pullout tests were used to determine the fiber/matrix interfacial frictional bond τ_0, interfacial chemical bond G_d and fiber slip-hardening coefficient β (Redon et al. [42]). The single fiber pullout test was conducted with a load cell with 44.48 N capacity at a loading rate of 0.01 mm/s. The fiber bridging law $\sigma(\delta)$ can be determined from the aforementioned micromechanical parameters. The complementary energy $J_b^{'}$ and fiber bridging capacity σ_0 were then deduced from the $\sigma(\delta)$ relation.

4. Results and discussion

4.1. Workability

Fig. 4 illustrates the effects of MgO proportion (in % PC replacement) on the workability of ECC with a fixed amount of superplasticizer (0.32% in binder mass), in terms of the flow time and flow diameter. Increased flow time and decreased flow diameter were observed for all specimens with increasing MgO proportion. To achieve similar fresh properties in all mixes, the proportion of superplasticizers was adjusted (Table 1). As expected, the superplasticizer content needed increased with increasing MgO proportion. This is attributed to the higher internal friction during mixing caused by the MgO particles that resulted in lower workability of ECC.

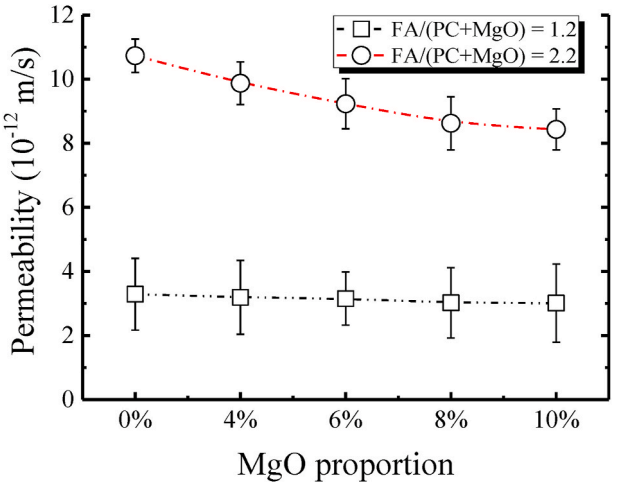

Fig. 6. Effect of MgO proportion on water permeability of ECC mixes.

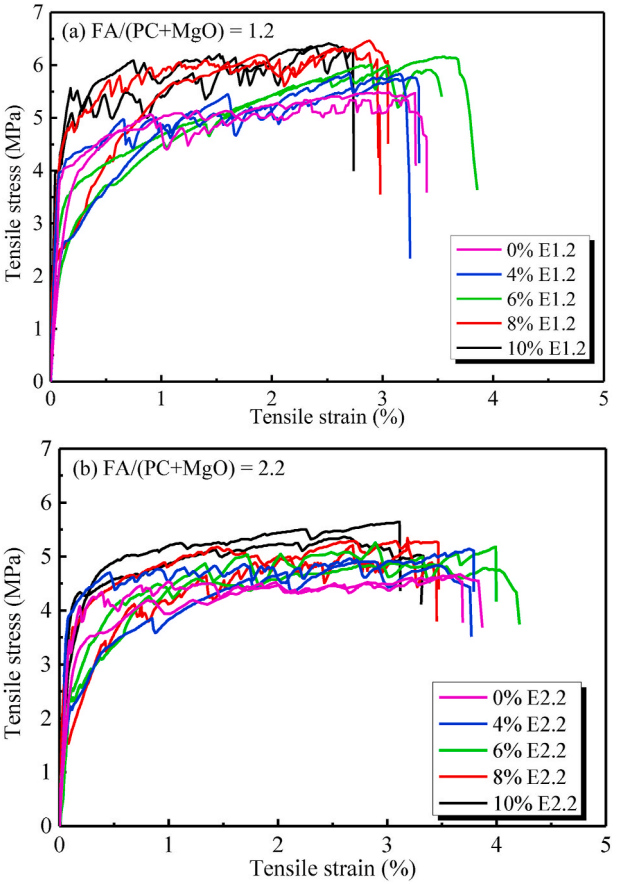

Fig. 7. Tensile performance of (a) FA/(PC + MgO) = 1.2; (b) FA/(PC + MgO) = 2.2.

4.2. Compressive strength and porosity

The influence of MgO proportion on the compressive strength and porosity for the two different batches of ECC are presented in Fig. 5. The compressive strength decreased with increasing MgO proportion (Fig. 5). As the MgO proportion increased from 0% to 6%, the compressive strength of E1.2 and E2.2 series slightly decreased from 52.8 to 49.3 and from 41.9 MPa to 37.6 MPa, respectively. The compressive strength dramatically decreased to 34.4 and 27.9 MPa for

Table 4
Summary of major tensile properties of MgO-doped ECC.

Series	MgO Proportion	First cracking strength (MPa)	Tensile strain capacity (%)	Ultimate tensile strength (MPa)
E1.2	0%	5.06 ± 0.15	3.35 ± 0.07	5.37 ± 0.14
	4%	4.45 ± 0.13	3.37 ± 0.05	5.77 ± 0.12
	6%	4.35 ± 0.06	3.61 ± 0.10	6.10 ± 0.07
	8%	4.25 ± 0.21	3.02 ± 0.04	6.33 ± 0.13
	10%	4.12 ± 0.11	2.73 ± 0.01	6.41 ± 0.08
E2.2	0%	4.29 ± 0.03	3.76 ± 0.11	4.64 ± 0.12
	4%	4.11 ± 0.12	3.83 ± 0.17	4.95 ± 0.08
	6%	3.63 ± 0.11	4.30 ± 0.18	5.11 ± 0.24
	8%	3.36 ± 0.08	3.41 ± 0.03	5.30 ± 0.04
	10%	3.23 ± 0.06	3.35 ± 0.05	5.52 ± 0.17

the ECC with 10% MgO. This decreased strength was likely due to the formation of brucite from the hydration of MgO, as the brucite is weaker than the C–S–H from cement hydration [43]. On the other hand, a higher proportion of MgO in ECC led to a lower porosity. As the MgO increased from 0% to 10%, the porosity was decreased by 14.1% and 8.2% for the E1.2 and E2.2 series, respectively. The lower matrix porosity was due to the expansive process of MgO hydration.

4.3. Permeability characteristic

Fig. 6 shows the measured permeability of ECC specimens as exposed to tap water. The water permeability decreases with increasing MgO proportion for both ECC series. As the MgO increased up to 10%, the permeability for the E1.2 and E2.2 series stabilized to 2.5×10^{-12} and 8.2×10^{-12} m/s, respectively. The reduction in permeability, especially for E2.2, is attributed to the decreased porosity caused by the expansion of MgO during hydration. In the presence of supersaturated Mg^{2+} and OH^{-}, the expansive $Mg(OH)_2$ is formed around the reaction site and filling the interior pores structures of ECC [10]. Nevertheless, a higher proportion of MgO in ECC has a relatively smaller effect on the permeability of the E1.2 as compared to E2.2. This is attributed to the high concentration of OH^{-} in the pores of E1.2 [10] leading to a shorter diffusion distance of Mg^{2+}. Thus, the expansive $Mg(OH)_2$ is formed locally at or in a confined region near the site of MgO particle but not fill well for the interior pores structures [44].

4.4. Tensile performance

Fig. 7 illustrates the tensile properties of MgO-doped ECC. The tensile stress at the initial crack was treated as the first cracking strength σ_{fc}, and the peak tensile stress was treated as the ultimate tensile strength σ_u. The tensile strain corresponding to σ_u was labelled as the ultimate tensile strain. These tensile properties for MgO-doped ECC are summarized in Table 4.

For the control mix (without MgO) in the E1.2 series, the first cracking strength σ_{fc} and ultimate tensile strength σ_u was 5.06 MPa and 5.37 MPa, respectively. Introducing MgO reduced the first cracking strength σ_{fc} by 18.6% but enhance the ultimate tensile strength up to 6.41 MPa. With MgO proportion ranging from 0% to 10%, the tensile strain capacity of the E1.2 series increased to 3.61% at the proportion of 6%, but then decreased to 2.73% at the proportion of 10%. The same trend was observed for these three properties for the E2.2 series, where the highest tensile strain capacity was 4.30% for the mix with 6% MgO and progressively decreased with higher proportion of MgO in ECC.

A typical crack pattern MgO-doped ECC is shown in Fig. 8. The imposed deformation of the specimen is largely caused by the multiple cracking under tension [45]. Table 5 shows the average crack number and residual crack width after unloading. Increasing MgO proportion reduced the average crack width but increased the crack number.

4.5. Fiber/matrix interfacial parameters

The composite behavior of MgO-doped ECC, especially the tensile behavior, can be further understood by inspecting the micromechanical properties as a function of MgO content. The measured micromechanical parameters, i.e., Young's modulus E_m, matrix fracture toughness K_m, interfacial frictional bond τ_0, interfacial chemical bond G_d and slip hardening coefficient β are presented in Figs. 9–11. The Young's modulus E_m and matrix fracture toughness K_m showed decreasing trends with increasing MgO proportion (Fig. 9).

The interfacial chemical bond G_d exhibits an overall decreasing trend with increasing MgO proportion for both ECC series, as shown in Fig. 10 (a). A lower interfacial chemical bond G_d means a weaker chemical adhesion between the PVA fibers and matrix, which could lead to an easier fiber/matrix interface debonding without the rupture of fiber. Generally, the fiber/matrix interfacial chemical bond G_d is believed to

Table 5
Crack parameters of ECC obtained on dumbbell-shaped specimens.

Series	MgO Proportion	Residual average crack width (μm)	Residual crack number
E1.2	0%	43.78	51
	4%	40.81	55
	6%	37.24	62
	8%	32.26	65
	10%	30.13	67
E2.2	0%	31.62	71
	4%	30.04	75
	6%	28.72	79
	8%	26.25	81
	10%	22.62	84

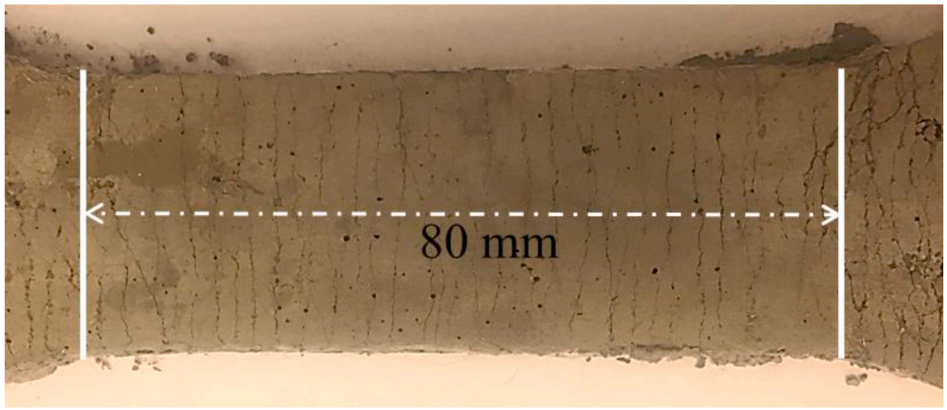

Fig. 8. Typical crack pattern of a E1.2 with 6% MgO specimen after 28 days curing.

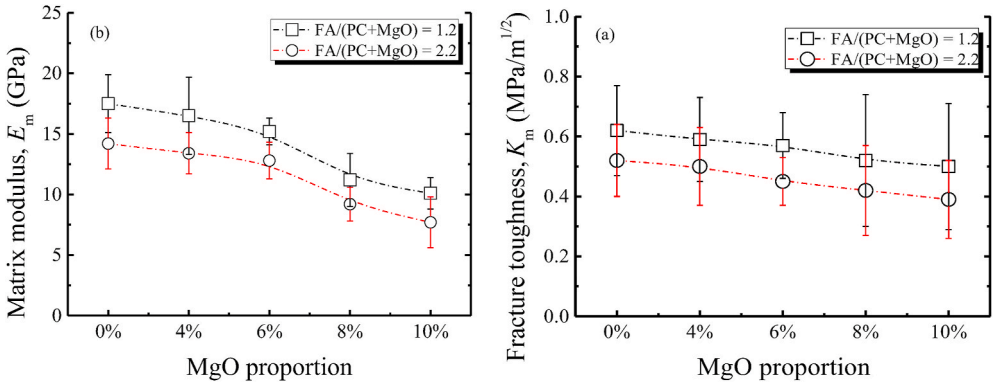

Fig. 9. Variations of (a) Young's modulus and (b) matrix fracture toughness in MgO-doped ECC.

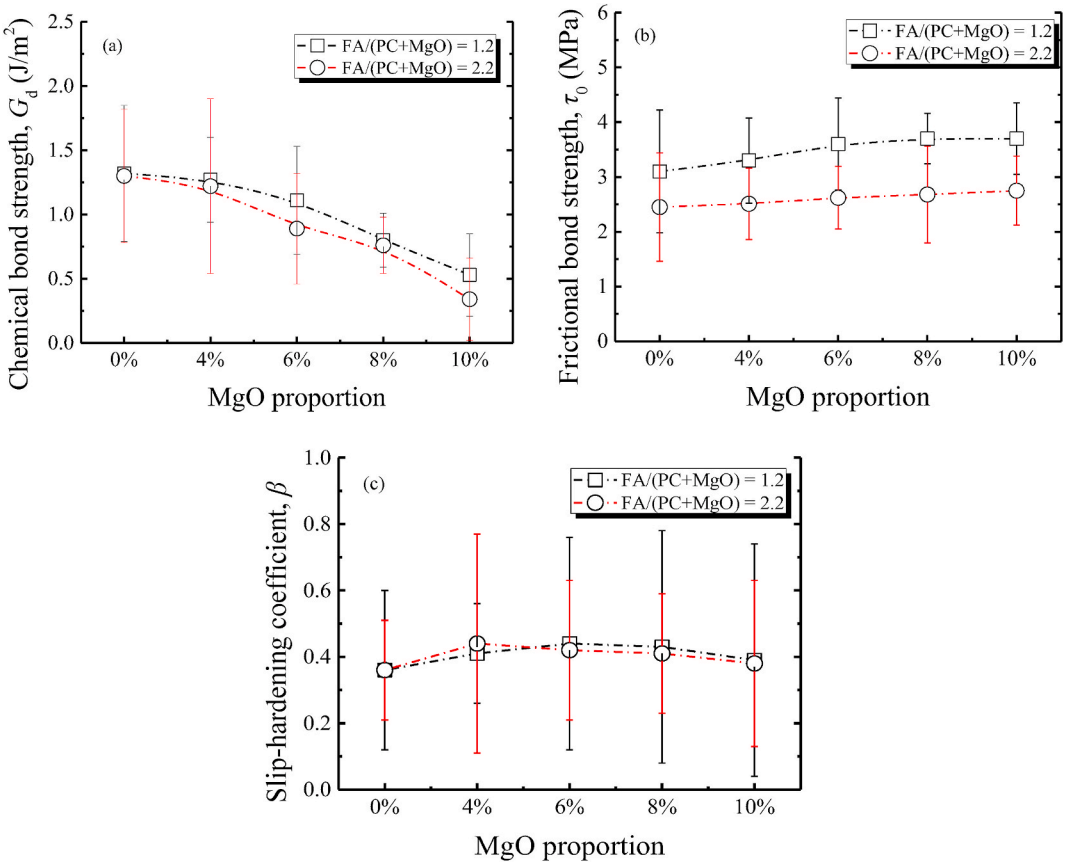

Fig. 10. Influence of MgO proportion on the fiber/matrix interfacial properties in ECC: (a) chemical bond G_d; (b) frictional bond τ_0; (c) slip-hardening coefficient β

be governed by the calcium hydroxide ($Ca(OH)_2$) layer [46]. The high proportion of MgO reduces the concentration of $Ca(OH)_2$, and diminishes the chemical bond. As compared to E1.2, the higher proportion of fly ash in E2.2 leads to lower G_d, which agrees well with previously reported results [45–47].

The frictional bond τ_0 is governed by the microstructure at the fiber/matrix interfacial transition zone. A higher frictional bond strength τ_0 indicates a denser microstructure in the interface and a higher resistance against fiber sliding. As shown in Fig. 10 (b), the increase of MgO proportion shows positive effects on the τ_0 due to the densification the microstructure (Fig. 5). The higher proportion of spherical fly ash particles (Fig. 1) with limited hydration is beneficial to fiber sliding, and therefore contributes to a lowerτ_0 [45,48,49].

The slip-hardening coefficient β describes the slip-dependent response of fiber during pulling-out from the matrix [46]. Lower slip-hardening coefficient β indicates less abrasion and delamination of the fiber embedded in the matrix. The MgO and fly ash proportions do not show obvious trends on the slip-hardening coefficient β (Fig. 10 (c)).

4.6. Micromechanical analysis

Fig. 11 shows the fiber bridging vs. crack opening relation from the micromechanical modeling, from which the complementary energy J_b' and the fiber bridging capacity σ_0 can be derived. The $\sigma(\delta)$ curve becomes steeper with increasing MgO proportion for both ECC series. The PSH(strength) and PSH(energy) (Eq. (3) and Eq. (4)) were computed and shown in Table 6.

It can be observed that the change in calculated fiber bridging capacity σ_0 is small (less than 2%), while first cracking strength σ_{fc}

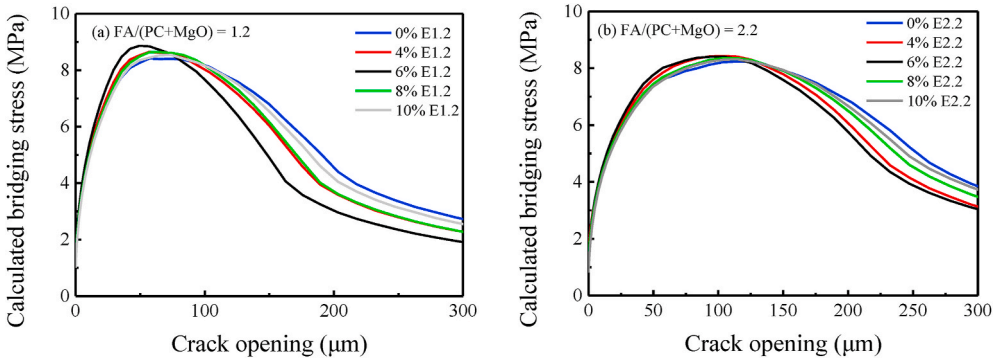

Fig. 11. Computed$\sigma(\delta)$ curve of ECC at various MgO proportion: (a) FA/(PC + MgO) = 1.2; (b) FA/(PC + MgO) = 2.2.

Table 6
Strain-hardening parameters for ECC mixes.

Series	MgO proportion	σ_0	σ_{fc}	σ_0/σ_{fc}	J_{tip}	J_b'	J_b'/J_{tip}
E1.2	0%	8.42	5.06	1.66	21.94	101.10	4.61
	4%	8.65	4.45	1.94	21.08	102.21	4.85
	6%	8.85	4.35	2.03	21.33	108.54	5.09
	8%	8.64	4.25	2.04	24.12	108.73	4.51
	10%	8.54	4.12	2.07	24.75	110.52	4.47
E2.2	0%	8.23	4.29	1.92	18.99	147.25	7.75
	4%	8.43	4.11	2.05	18.62	147.86	7.92
	6%	8.41	3.63	2.32	15.73	148.68	9.45
	8%	8.35	3.36	2.49	19.21	149.22	7.80
	10%	8.31	3.23	2.57	19.82	152.31	7.72

dropped by as much as 19% for E1.2 and 25% for E2.2, as the increase of MgO proportion from 0% to 10%. The correlation between PSH index and ultimate tensile strength is depicted in Fig. 12 (a). The increasing trend of PSH in strength (Eqn. (3)) is consistent with the rising trend of ultimate tensile strength with increasing content of MgO. As the MgO proportion increased from 0% to 10%, it was observed the σ_0/σ_{fc} increased from 1.66 to 2.07 in the E1.2 test series, and from 1.92 to 2.57 in the E2.2 test series.

It can be seen that the crack tip toughness J_{tip} and the complementary energy J_b' have a gradual increase with increasing MgO proportion. The relation between the PSH(energy) index and the tensile strain capacity was illustrated in Fig. 12 (b). The observed maximum tensile strain capacity at the 6% MgO content is consistent with the highest PSH index for energy at the same MgO content, for both ECC series. Thus, a larger margin between J_b' and J_{tip} enhances the probability of saturated multiple cracking with 6% MgO replacement of PC in ECC. The mechanism of the optimal effect of 6% MgO on the composite properties of ECC is summarized in Fig. 13. Consequently, a robust tensile ductility in ECC could be obtained by substituting 6% of Portland cement with MgO.

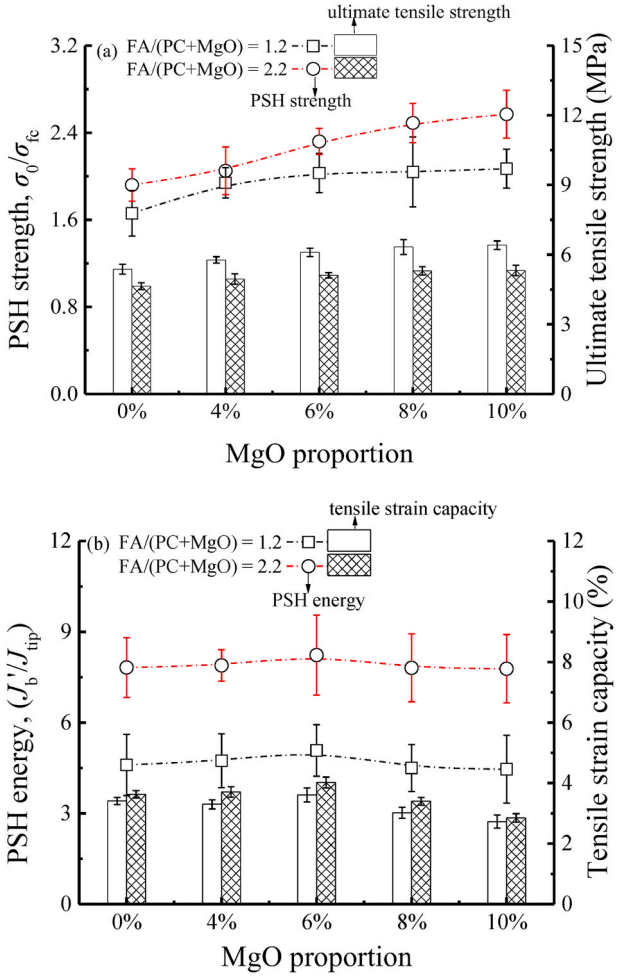

Fig. 12. PSH strength and PSH energy correlation with MgO proportion for ECC mixes: (a) PSH strength and ultimate tensile strength; (b) PSH energy and tensile strain capacity.

5. Conclusions

This study focused on the changes in composite properties, including workability, compressive strength, permeability and tensile performance, as well as micromechanical behavior of ECC with OPC partially replaced by MgO. Changes in composite tensile properties were traced to the micromechanical properties altered by the introduction of MgO. The following conclusions can be drawn:

(1) With partial substitution of OPC by MgO, changes in mechanical, physical, and fresh properties of ECC were observed. Specifically, a lower first cracking strength and compressive strength in the MgO-ECC were found. This is because the brucite reaction product resulting from MgO had a smaller contribution to strength as compared to C–S–H from cement hydration. The introduction of MgO in ECC tended to densify the microstructure through the formation of expansive brucite, leading to a lower permeability of 3.0×10^{-12} - 1.1×10^{-11} cm/s. However, the decrease depended on the FA content of the ECC. The permeability reduction was more significant for the E2.2 mix with higher FA content than E1.2. Furthermore, a higher MgO content in ECC created higher internal friction during mixing and resulted in a lower workability of the fresh ECC.

(2) At the macro-composite level, robust and tensile strain-hardening were observed in the MgO-doped ECC. An increase of MgO

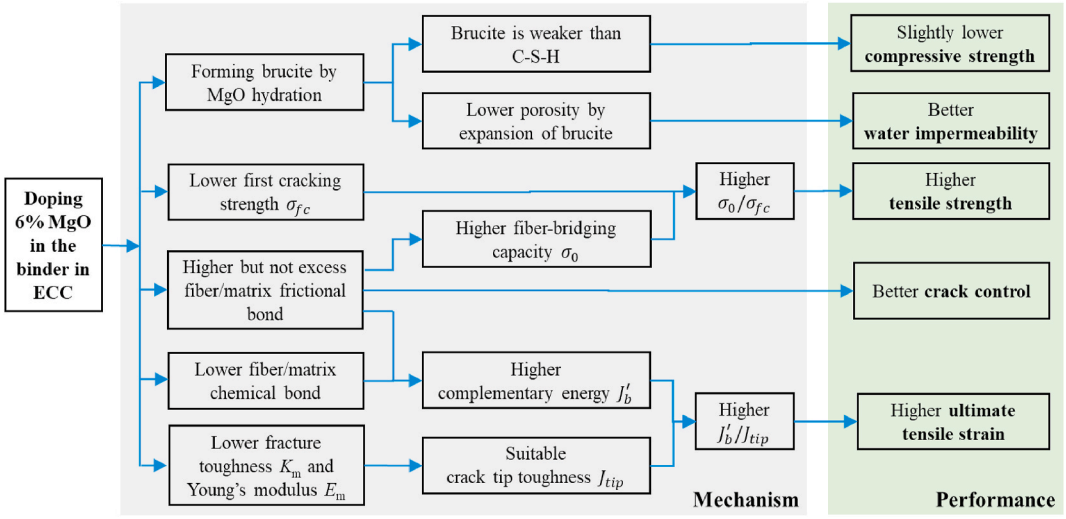

Fig. 13. Effect of substituting 6% cement by MgO on composite properties of ECC.

content generally reduce the average crack width, and led to an increase in the ultimate tensile strength and the crack number. The ultimate tensile strain up to 4.3% was obtained in the ECC with 6% replacement of OPC by MgO.

(3) At the composite matrix level, a higher MgO proportion tended to reduce the Young's modulus E_m and the matrix fracture toughness K_m because of the weak bonding of the brucite phase in the matrix. At the fiber/matrix interface level, MgO tended to increase the frictional bond strength τ_0 and reduce the interfacial chemical bond G_d. These changes led to a continuous rise in the σ_0/σ_{fc} ratio with increase in MgO content, and a maximum J_b'/J_{tip} ratio at 6% MgO replacement of OPC.

(4) The correlation between the maximum tensile strain capacity at the macro-composite level and a maximum J_b'/J_{tip} ratio found at 6% MgO replacement of OPC suggests that an optimal tuning of the fiber/matrix and matrix parameters in ECC was achieved by moderate lowering of the matrix toughness in combination with enhancement of fiber bridging behavior, consistent with the expectation from micromechanical model on tensile strain-hardening in ECC.

The findings of this study warrant further research on the long-term mechanical performance of MgO-doped ECC in the field. In addition, future investigation on material microstructures of MgO-doped ECC should shed light on the physical mechanisms responsible for the observations made on the matrix and fiber/matrix interface.

Declaration of competing interest

The authors declare that they have no known competing financial interests or personal relationships that could have appeared to influence the work reported in this paper.

Acknowledgments

This study was partially supported by a grant to the University of Michigan from the US National Science Foundation (CMMI-1634694) and by the James R. Rice Distinguished University Professorship. Hao-Liang Wu acknowledges the support from the Chinese Scholarship Council, which enabled his visit the Advanced Civil Engineering Materials Research Laboratory (ACE-MRL) at the University of Michigan.

References

[1] V.C. Li, D.K. Mishra, A.E. Naaman, J.K. Wight, J.M. LaFave, H.C. Wu, Y. Inada, On the shear behavior of engineered cementitious composites, Adv. Cement Base Mater. 1 (3) (1994) 142–149.
[2] V.C. Li, Introduction to Engineered Cementitious Composites (ECC), Springer Berlin Heidelberg, 2019, pp. 1–10, https://doi.org/10.1007/978-3-662-58438-5_1.
[3] J. Yu, Y. Chen, C.K.Y. Leung, Mechanical performance of Strain-Hardening Cementitious Composites (SHCC) with hybrid polyvinyl alcohol and steel fibers, Compos. Struct. 226 (2019) 111198, https://doi.org/10.1016/j.compstruct.2019.111198.
[4] D. Zhang, H.L. Wu, V.C. Li, B.R. Ellis, Autogenous healing of Engineered Cementitious Composites (ECC) based on MgO-fly ash binary system activated by carbonation curing, Construct. Build. Mater. 238 (2020) 117672, https://doi.org/10.1016/j.conbuildmat.2019.117672.
[5] H.L. Wu, J. Yu, D. Zhang, J.X. Zheng, V.C. Li, Effect of morphological parameters of natural sand on mechanical properties of engineered cementitious composites, Cement Concr. Compos. 100 (2019) 108–119, https://doi.org/10.1016/j.cemconcomp.2019.04.007.
[6] M.D. Lepech, V.C. Li, Water permeability of engineered cementitious composites, Cement Concr. Compos. 31 (10) (2009) 744–753, https://doi.org/10.1016/j.cemconcomp.2009.07.002.
[7] D. Zhang, J. Yu, H. Wu, B. Jaworska, B.R. Ellis, V.C. Li, Discontinuous micro-fibers as intrinsic reinforcement for ductile Engineered Cementitious Composites (ECC), Compos. B Eng. (2020) 107741, https://doi.org/10.1016/j.compositesb.2020.107741.
[8] J. Yu, H.L. Wu, C.K. Leung, Feasibility of using ultrahigh-volume limestone-calcined clay blend to develop sustainable medium-strength Engineered Cementitious Composites (ECC), J. Clean. Prod. (2020) 121343.
[9] J. Yu, J. Yao, X. Lin, H. Li, J.Y. Lam, C.K. Leung, M.L. Ivan, K. Shih, Tensile performance of sustainable Strain-Hardening Cementitious Composites with hybrid PVA and recycled PET fibers, Cement Concr. Res. 107 (2018) 110–123, https://doi.org/10.1016/j.cemconres.2018.02.013.
[10] H. Liu, Q. Zhang, C. Gu, H. Su, V.C. Li, Influence of micro-cracking on the permeability of engineered cementitious composites, Cement Concr. Compos. 72 (2016) 104–113, https://doi.org/10.1016/j.cemconcomp.2016.05.016.
[11] H.L. Wu, Y.J. Du, J. Yu, Y.L. Yang, V.C. Li, Hydraulic conductivity and self-healing performance of engineered cementitious composites exposed to acid mine drainage, Sci. Total Environ. (2020) 137095, https://doi.org/10.1016/j.scitotenv.2020.137095.
[12] H.L. Wu, D. Zhang, Y.J. Du, V.C. Li, Durability of engineered cementitious composite exposed to acid mine drainage, Cement Concr. Compos. (2020) 103550, https://doi.org/10.1016/j.cemconcomp.2020.103550.
[13] M. Kunieda, K. Rokugo, Recent progress on HPFRCC in Japan, J. Adv. Concr. Technol. 4 (1) (2006) 19–33, https://doi.org/10.3151/jact.4.19.
[14] S. Qian, M.D. Lepech, Y.Y. Kim, V.C. Li, Introduction of transition zone design for bridge deck link slabs using ductile concrete, ACI Struct. J. 106 (1) (2009), https://doi.org/10.14359/56288.
[15] V. Mechtcherine, Novel cement-based composites for the strengthening and repair of concrete structures, Construct. Build. Mater. 41 (2013) 365–373, https://doi.org/10.1016/j.conbuildmat.2012.11.117.
[16] B.T. Huang, Q.H. Li, S.L. Xu, B. Zhou, Strengthening of reinforced concrete structure using sprayable fiber-reinforced cementitious composites with high ductility, Compos. Struct. 220 (2019) 940–952, https://doi.org/10.1016/j.compstruct.2019.04.061.

[17] S. Ruan, J. Qiu, E.H. Yang, C. Unluer, Fiber-reinforced reactive magnesia-based tensile strain-hardening composites, Cement Concr. Compos. 89 (2018) 52–61, https://doi.org/10.1016/j.cemconcomp.2018.03.002.
[18] H.L. Wu, F. Jin, Y.L. Bo, Y.J. Du, J.X. Zheng, Leaching and microstructural properties of lead contaminated kaolin stabilized by GGBS-MgO in semi-dynamic leaching tests, Construct. Build. Mater. 172 (2018) 626–634, https://doi.org/10.1016/j.conbuildmat.2018.03.164.
[19] J. Yu, H.L. Wu, D.K. Mishra, G. Li, C.K.Y. Leung, Compressive strength and environmental impact of sustainable blended cement with high-dosage Limestone and Calcined Clay (LC2), J. Clean. Prod. (2020) 123616, https://doi.org/10.1016/j.jclepro.2020.123616.
[20] C. Du, A review of magnesium oxide in concrete, Concr. Int. 27 (12) (2005) 45–50.
[21] S.A. Walling, J.L. Provis, Magnesia-based cements: a journey of 150 years, and cements for the future, Chem. Rev. 116 (7) (2016) 4170–4204, https://doi.org/10.1021/acs.chemrev.5b00463.
[22] M.A. Sherir, K.M. Hossain, M. Lachemi, The influence of MgO-type expansive agent incorporated in self-healing system of engineered cementitious Composites, Construct. Build. Mater. 149 (2017) 164–185, https://doi.org/10.1016/j.conbuildmat.2017.05.109.
[23] M.A. Sherir, K.M. Hossain, M. Lachemi, Self-healing and expansion characteristics of cementitious composites with high volume fly ash and MgO-type expansive agent, Construct. Build. Mater. 127 (2016) 80–92, https://doi.org/10.1016/j.conbuildmat.2016.09.125.
[24] H.L. Wu, D. Zhang, B.R. Ellis, V.C. Li, Development of reactive MgO-based Engineered Cementitious Composite (ECC) through accelerated carbonation curing, Construct. Build. Mater. 191 (2018) 23–31, https://doi.org/10.1016/j.conbuildmat.2018.09.196.
[25] C.J. Shi, Y.Y. Li, Investigation on some factors affecting the characteristics of alkali-phosphorus slag cement, Cement Concr. Res. 19 (4) (1989) 527–533, https://doi.org/10.1016/0008-8846(89)90004-5.
[26] M.B. Haha, B. Lothenbach, G.L. Le Saout, F. Winnefeld, Influence of slag chemistry on the hydration of alkali-activated blast-furnace slag-Part I: effect of MgO, Cement Concr. Res. 41 (9) (2011) 955–963, https://doi.org/10.1016/j.cemconres.2011.05.002.
[27] T.S. Qureshi, A. Al-Tabbaa, Self-healing of drying shrinkage cracks in cement-based materials incorporating reactive MgO, Smart Mater. Struct. 25 (8) (2016), 084004, https://doi.org/10.1088/0964-1726/25/8/084004.
[28] J. Qiu, S. Ruan, C. Unluer, E.H. Yang, Autogenous healing of fiber-reinforced reactive magnesia-based tensile strain-hardening composites, Cement Concr. Res. 115 (2019) 401–413, https://doi.org/10.1016/j.cemconres.2018.09.016.
[29] S. Ruan, C. Unluer, Comparative life cycle assessment of reactive MgO and Portland cement production, J. Clean. Prod. 137 (2016) 258–273, https://doi.org/10.1016/j.jclepro.2016.07.071.
[30] C. Unluer, A. Al-Tabbaa, Impact of hydrated magnesium carbonate additives on the carbonation of reactive MgO cements, Cement Concr. Res. 54 (2013) 87–97, https://doi.org/10.1016/j.cemconres.2013.08.009.
[31] V.C. Li, C.K.Y. Leung, Steady-state and multiple cracking of short random fiber composites, J. Eng. Mech. 118 (11) (1992) 2246–2264, https://doi.org/10.1061/(asce)0733-9399(1992)118:11(2246).
[32] E.H. Yang, S. Wang, Y. Yang, V.C. Li, Fiber-bridging constitutive law of engineered cementitious composites, J. Adv. Concr. Technol. 6 (1) (2008) 181–193, https://doi.org/10.3151/jact.6.181.
[33] Y. Wang, L. Wei, J. Yu, et al., Mechanical properties of high ductile magnesium oxychloride cement-based composites after water soaking, Cement Concr. Compos. 97 (2019) 248–258.
[34] L. Wei, Y. Wang, J. Yu, et al., Feasibility study of strain hardening magnesium oxychloride cement-based composites, Construct. Build. Mater. 165 (2018) 750–760.
[35] T. Kanda, V.C. Li, Practical design criteria for saturated pseudo strain hardening behavior in ECC, J. Adv. Concr. Technol. 4 (1) (2006) 59–72, https://doi.org/10.3151/jact.4.59.
[36] ASTM C150/C150M, Standard Specification for Portland Cement, ASTM International, West Conshohocken, PA, USA, 2016.
[37] ASTM C618/C618M, Standard Specification for Coal Fly Ash and Raw or Calcined Natural Pozzolan for Use in Concrete, ASTM International, West Conshohocken, PA, USA, 2012.
[38] M. Li, V.C. Li, Rheology, fiber dispersion, and robust properties of engineered cementitious composites, Mater. Struct. 46 (3) (2013) 405–420, https://doi.org/10.1617/s11527-012-9909-z.
[39] ASTM, C109/C109M, Standard Test Method for Compressive Strength of Hydraulic Cement Mortars (Using 2-in. Or [50-mm] Cube Specimens), ASTM International, West Conshohocken, PA, 2013.
[40] JSCE, Recommendations for Design and Construction of High Performance Fiber Reinforced Cement Composites with Multiple Fine Cracks (HPFRCC), 2008. Tokyo.
[41] ASTM, E399, Standard Test Method for Linear-Elastic Plane-Strain Fracture Toughness KIc of Metallic Materials, ASTM International, West Conshohocken, PA, USA, 2012.
[42] C. Redon, V.C. Li, C. Wu, H. Hoshiro, T. Saito, A. Ogawa, Measuring and modifying interface properties of PVA fibers in ECC matrix, Title J Mater Civ Eng 13 (6) (2001) 399–406, https://doi.org/10.1061/(asce)0899-1561(2001)13:6(399).
[43] C. Unluer, Carbon dioxide sequestration in magnesium-based binders, in: Carbon Dioxide Sequestration in Cementitious Construction Materials, 2018, pp. 129–173, https://doi.org/10.1016/b978-0-08-102444-7.00007-1.
[44] L. Mo, M. Deng, M. Tang, et al., Effects of calcination condition on expansion property of MgO-type expansive agent used in cement-based materials, Cement Concr. Res. 40 (3) (2010) 437–446.
[45] E.H. Yang, Y. Yang, V.C. Li, Use of high volumes of fly ash to improve ECC mechanical properties and material greenness, ACI Mater. J. 104 (6) (2007) 620, https://doi.org/10.14359/18966.
[46] Y.W. Chan, Fiber/Cement Bond Property Modification in Relation to Interfacial Microstructure, Department of Civil and Environmental Engineering, University of Michigan, Ann Arbor, MI, 1994.
[47] H. Ma, S. Qian, Z. Zhang, Z. Lin, V.C. Li, Tailoring engineered cementitious composites with local ingredients, Construct. Build. Mater. 101 (2015) 584–595, https://doi.org/10.1016/j.conbuildmat.2015.10.146.
[48] S. Wang, V.C. Li, Engineered cementitious composites with high-volume fly ash, ACI Mater. J. 104 (3) (2007) 233–241, https://doi.org/10.14359/18668.
[49] J. Yu, H. Li, C.K.Y. Leung, Matrix design for waterproof engineered cementitious composites (ECC), Construct. Build. Mater. 139 (2017) 438–446, https://doi.org/10.1007/978-3-662-58438-5_2.